ELSEVIER

Journal of Magnetism and Magnetic Materials 148 (1995) 446–454

Journal of magnetism and magnetic materials

Microscopic imaging of recorded patterns subjected to an external dc erasing magnetic field

Romel D. Gomez [a,b,*], Rajiv Madabhushi [a], Isaak D. Mayergoyz [a], Laura J. Lising [b,1], Edward R. Burke [b]

[a] *Department of Electrical Engineering, University of Maryland, College Park, MD 20742, USA*
[b] *Laboratory for Physical Sciences, 8050 Greenmead Drive, College Park, MD 20740, USA*

Abstract

Magnetic structures in thin-film recording media were imaged with sub-micron resolution while undergoing dc erasure. Distinct changes in the patterns occurred at applied fields as low as 150 Oe below the media coercivity, and characteristic spatial variations were observed with applied fields approaching and extending beyond the coercivity. The results show that the onset of erasure is initiated by the rotation of magnetic moments at the track edges. As the field is increased, the regions magnetized parallel to the applied field expand in the direction of the field while those oriented antiparallel to it contact. Above the coercivity the unfavorably magnetized areas break up into remnant clusters whose sizes decrease as the entire region coalesces into a single magnetization structure. This paper correlates these microscopic results with macroscopic measurements of the medium and suggests possible mechanisms that lead to data erasure through media saturation.

1. Introduction

No treatment of erasure in magnetic memory systems would be complete without direct scrutiny of their microscopic behavior. At present, the bulk of theoretical and experimental work [1–7] on erasure deals with performance issues attributable to macroscopic properties. The purpose of this work is to supplement those findings by focusing on the microscopic behavior of magnetic patterns as their moments progressively realign with the external dc erasure field. We exploit the newly developed capability for imaging magnetic patterns with high resolution to observe changes in the local magnetization distribution. The behavior is correlated with specific points along the measured remanence curves, thus providing significant insight into the mechanisms that lead to data erasure. Specifically, our interest is to establish (i) whether there exists a sequential order that governs the switching of specific areas on the track, (ii) the behavior of the transition zones as the magnetizations are either reversed or reinforced by the external field, (iii) the role played by the demagnetization field in wavelength-dependent erasure characteristics, and (iv) the residual distribution of magnetic islands at the final stages of erasure. In addition, based upon the knowledge of the interparticle interactions of the medium, we attempt to interpret the observed behavior in terms of the switching of magnetic moments.

* Corresponding author. Fax: +1-301-935-6723; email: romel_d_gomez@umail.umd.edu.

[1] Present address: Physics Department, University of California at Berkeley, CA 94720, USA.

SSDI 0304-8853(95)00083-6

2. Experimental technique

The large-scale magnetic properties of the medium were measured using a vibrating sample magnetometer (VSM) with a nickel standard sphere used in converting from M–H to B–H plots. Plots of the major loops of the B–H curve, the dc demagnetization and isothermal remanence curves were acquired for the medium. Any given point on the dc demagnetization curve represents the remanent magnetization after saturating the medium with a large positive field and then applying a negative demagnetizing field. Points on the isothermal remanence curve, on the other hand, were obtained by initially placing the medium in an unmagnetized state (by ac demagnetization) and observing the remanent magnetization after applying a positive dc field. A measure of the exchange interaction between the grains in the medium, commonly referred to as the δM curve, can be derived from these two sets of data. The δM values represent the departure of the medium from the perfectly non-interacting distribution of particles described by the Stoner–Wohlfarth model and calculated as [8]:

$$\delta M = I_d(H) + 2I_r(H) - 1, \qquad (1)$$

where $I_d(H)$ and $I_r(H)$ are the demagnetization and isothermal remanence magnetizations normalized relative to the saturation magnetization.

Local characterization of the erasure process was studied by producing a series of spatially resolved magnetic field images of a particular section of a thin-film rigid-disk medium and sequentially observing the remanent patterns as the field is increased. Images of the magnetic field distributions of surface patterns were obtained by using our magnetic force scanning tunneling microscope [9]. In essence, this method modifies a scanning tunneling microscope by replacing the tip with a free-standing magnetic thin-film probe. As with a normal STM, this probe is rastered across the surface as a feedback system continuously adjusts the vertical position to maintain constant current. In contrast with the standard STM, however, the interaction with the surface magnetic field deflects the probe, which also introduces variations in the tunneling current. Hence, this modified STM effectively yields a two-dimensional array of changes in z as a function of the lateral position, $\Delta z(x, y)$, which reflects contributions from both magnetic features as well as surface morphology. The response of the probe associated with the magnetic interaction has been calculated by using a simple 'point charge' model for the probe [10]. The variation in the vertical displacement $\Delta z(x, y)$ was shown to be directly proportional to the individual components of the field, i.e. [11]

$$\Delta z \propto \left(\hat{p} \cdot \vec{H}_{\parallel}\right) \sin\theta \cos\theta + H_{\perp} \sin^2\theta, \qquad (2)$$

where $\hat{p}$ is a unit vector in the direction of the probe projection on the surface plane, and θ is the inclination angle made by the probe and the surface normal. The contrast mechanism can thus be interpreted as arising from the contributions of the vertical component $H_{\perp}$ of the local surface field as well as the corresponding in-plane component $\vec{H}_{\parallel}$ in the direction of $\hat{p}$ at a fixed height above the surface. In addition, by appropriately adjusting the geometrical parameters θ and $\hat{p}$, selective imaging of any specific field component can be performed.

In order to introduce an external field to the sample, the instrument was further modified to accept an electromagnetic yoke having a small (3 mm) gap at the sample position. The intensity of the field at the gap has been varied by adjusting the current on the 3400-turn solenoid. With this design, the field was assumed to be horizontal and uniform within the 65×65 μm imaging spot. The average field at the sample position was measured using a miniature Hall probe with a 125×125 μm active area which was calibrated against the vibrating sample magnetometer. The geometry was arranged such that the direction of the dc field was along the surface plane and parallel to the pattern track direction. The sample was prepared from a formatted commercial thin-film hard disk and was cut into small pieces to fit the modified STM. The sample was then processed by following the prescribed preparation procedures to enhance tunneling between the surface and the probe [12].

Data collection was performed as follows: The external dc magnetic field was slowly increased up to a given value, held there for about 20 s, slowly ramped back to zero, and then the corresponding magnetic images were taken. This procedure was repeated with progressively increasing fields. A set

of data on a single area comprised about 100–120 scanned images taken with about a 15 Oe increment near the coercive field. Care was taken to ensure that the magnetization of the probe was unaltered by the external fields. The probe was removed from the assembly during each application of the field. The images were shown successively at video rates in correct field order, which facilitated observation of the pattern evolution.

3. Results

3.1. Macroscopic characterization

The macroscopic properties of the media are summarized in Fig. 1. In the track direction, the coercivity $H_c(\text{par}) = 926$ Oe, $M_r\delta(\text{par}) = 5.0$ memu/cm^2, $S = 0.81$, and $S^* = 0.86$. Along the perpendicular (or cross-track) direction, $H_c(\text{per}) = 600$ Oe, and $M_r\delta(\text{per}) = 3.3$ memu/cm^2. The measure of relative in-plane anisotropy, defined by the orientation ratio $M_r(\text{par})/M_r(\text{per})$ is 1.50. The dashed line in Fig. 1(a) depicts the standard demagnetization remanence curve and although unresolved in the plot, the dc demagnetization coercivity is 934 Oe, which is about 8 Oe higher than the coercivity of the medium. The various points labeled along the remanence curve denote the respective locations where corresponding real-space images of the patterns are shown in Fig. 2. The δM curve for this medium is shown in Fig. 1(b), together with the points corresponding to its erasure state in Fig. 2. The positive peak of this curve indicates that the grains exhibit positive or stabilizing interparticle interaction, which implies that this medium favors magnetization as induced by external dc fields.

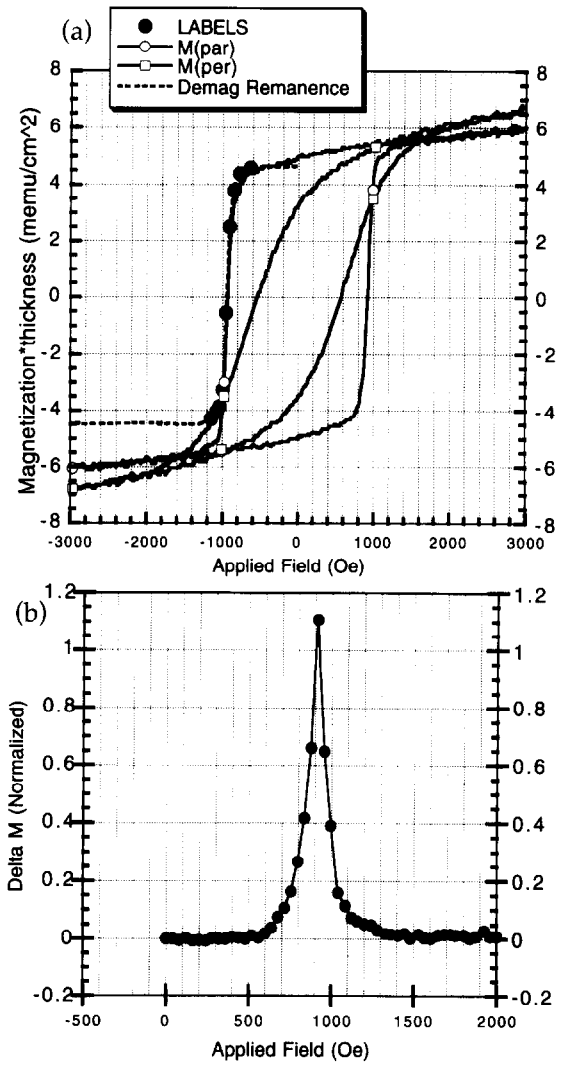

Fig. 1. Macroscopic properties of the sample. (a) Solid lines: magnetization curves along the parallel and perpendicular to track directions, dashed line: dc demagnetization remanence curve with labels corresponding to images in Fig. 2. (b) Measured δM curve (see text).

3.2. Microscopic characterization

The evolution of the remanent magnetization patterns after applying progressively increasing fields is exhibited in Fig. 2. In these magnetic field images, the probe was oriented such that the inclination angle θ is about 30° and the $\vec{p}$ is nominally along the track direction. From Eq. (2), the contrast arises primarily from the H_x contribution or the component of the field parallel to the surface and along the direction of the track, as well as a slight admixture of the normal component H_z. The series of repetitive alternating intensity represents the ordered series of alternating magnetization directions. These patterns are assumed to lie exclusively in the plane of the medium so that there is no component in the normal direction, i.e. $M_z = 0$. Furthermore, since the H_x contribution closely resembles the field-producing component of

the magnetization, we can treat the spatial variations as those of the surface magnetization.

Image 2A was taken at ambient (earth's) field after subjecting the sample to about 638 Oe. This is representative of the initial state of the system which is essentially unchanged from zero applied field up to about 700 Oe. This particular combination of short and long bit lengths is a common arrangement of a formatted commercial hard disk. Three distinct tracks are visible within the scan area of about 65×65 μm and are separated by bands along the edges. Emphasis was placed on establishing the lengths of the separation band, the track width, as well as the effective lengths of the bright and dark contrast areas. As far as the separation band width is concerned, the delineation between the edge of the track and the guard band is gradual and may cause ambiguity in measuring the widths. Nevertheless, the width of the bands is defined as the distance separating two adjacent tracks at half of their amplitudes. In this case, the average width is 3 μm. The width of the tracks themselves, defined in a similar fashion, has an average of about 19 μm. The spacing between transitions or bit lengths was also defined as the distance separating two transitions at their midpoints. There appears to be two distinct bit lengths

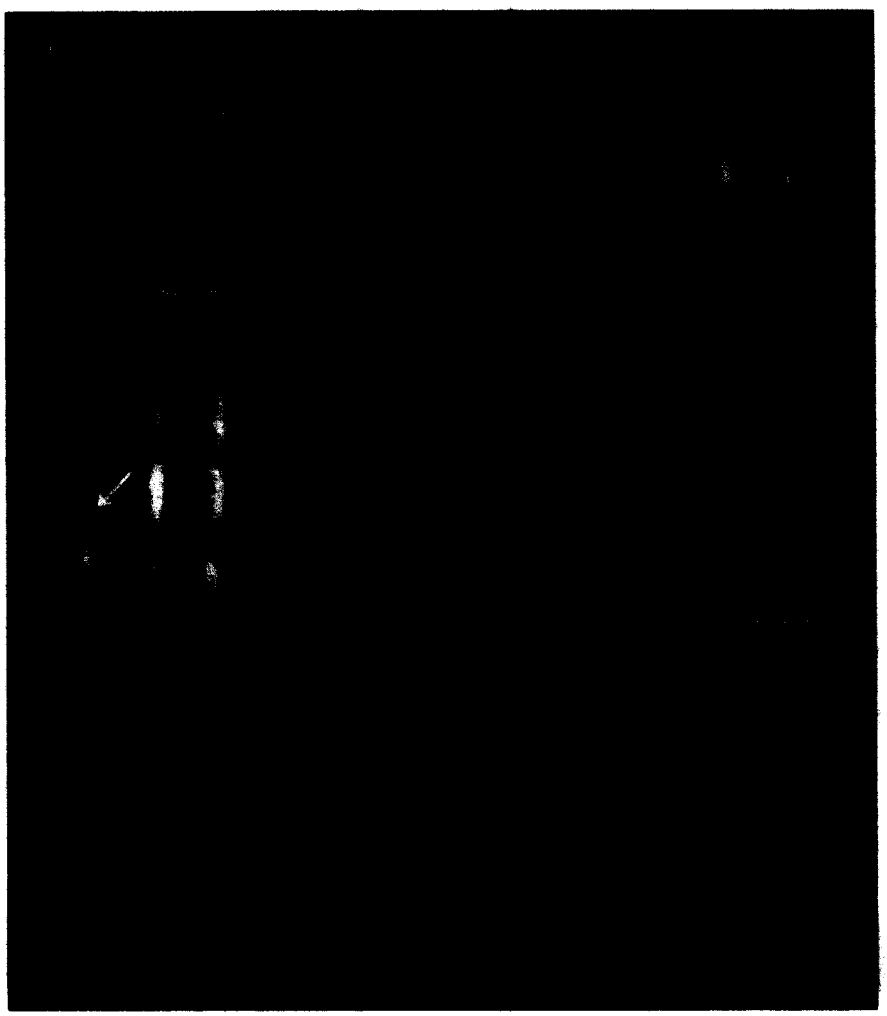

Fig. 2. Microscopic evolution of recorded thin-film patterns as progressively increasing dc field is applied.

for each magnetization direction: the long variety (L_1) in the middle of the image is twice the length of the short ones (L_2). Furthermore, the bright patterns appear to be generally longer than the dark patterns. On average, the long bright bit length is about 7 μm and the shorter bright pattern is 3.5 μm, while the dimensions are about 5 μm and 2.1 for the dark contrast areas, respectively.

Images B–D, obtained at fields below the coercivity, show some characteristic signs of the onset of erasure. In addition to the reduction in the intensity of the patterns, increasing the field has the effect of widening the guard bands. This is slowly varying between successive images, although an identifiable widening can be observed as early as 787 Oe in B. Comparison of Figs. 2A and 2D shows that the width of the bands has increased to about 8 μm at 913 Oe or a 5 μm increase from its initial value. This behavior is, of course, related to the trackwidths themselves being shortened. The trackwidth on average has decreased from its initial value of 19 μm in Fig. 2A down to about 14 μm in Fig. 2D, reflecting a similar 5 μm reduction within this 150 Oe range. Apart from this effect, we can similarly observe a characteristic variation in the bit lengths of the patterns with increasing field. Specifically, there appears to be a widening of the dark areas along the direction of the track which is accompanied by the shrinkage of the adjacent bright contrast areas. This takes place in all the tracks, but for the sake of clarity, brackets in the images focus on a specific region where the effect is conspicuous. Between Figs. 2A–D, the bit length of the dark area increased from 3 μm in A to about 6 μm in D, while the bit length of the bright area reduced from 8 to 5 μm. To recapitulate, images A–D demonstrate specific changes accompanying the onset of pattern erasure occurring at fields below the coercivity.

Figs. 2D and E show the behavior as the coercive field was traversed. We observe a more drastic reduction in pattern amplitude within this 50 Oe field range as compared with the cumulative effect of all the previous magnetic field exposures. The transition regions become less distinct as the boundaries begin to meander across the track. For fields at or above H_c, the most dominant effect does not appear to be the continued reduction of the track width nor the growth of specific favorable areas but the switching of individual clusters in various parts of the medium. An example of this phenomenon is marked by arrows in Figs. D and E. A cluster that was previously present in D has disappeared in E, while the adjacent cluster on the same bit has still clearly persisted. With any given field, a certain number of the moments switch, leaving a distribution of unswitched magnetic islands. The number of these islands continued to diminish, as shown in images F–G, but a substantial external field strength (greater than 1300 Oe) was required to eliminate completely all traces of magnetic structures below the detection sensitivity.

4. Discussion

4.1. Amplitude reduction

During the initial stages, the contrast decreases since the discontinuity in $\boldsymbol{M}$ between the two different regions decreases as the unfavorably magnetized areas gradually reorient themselves in the direction of the field. The dc field forces a particular magnetization to reverse while keeping the complementary magnetization, assumed to be at remanence, largely unperturbed. A quantitative summary of this behavior is depicted in Fig. 3, where the amplitudes for both the long and short bit length patterns are shown, as well as a section of the dc demagnetization remanence. These amplitudes were averaged over the central section of the track so that effects due to trackwidth reduction has been eliminated. At the initial state or when $H \approx 0$, the short bit patterns (L_2) were about 20% smaller than the corresponding long-wavelength patterns (L_1). This may be due to the intrinsic difference in the field strengths between the long- and short-wavelength patterns. In other words, the media may be equally saturated regardless of the wavelength but the measured magnetic field at a fixed height above the surface is weaker for the short-wavelength patterns. Alternatively, the difference may be regarded as the unability of the recording head to completely saturate the recording medium in writing the short wavelength patterns. The large demagnetization fields generated by the short-wavelength patterns as well as the reduced efficiency of the head at higher frequencies combine to hinder the

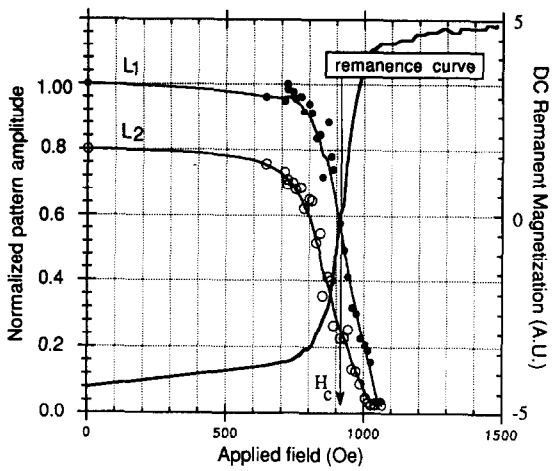

Fig. 3. Profile amplitude reduction with increasing applied fields for both long and short bit length patterns.

formation of these short-wavelength patterns. As the field is increased, the short-wavelength patterns diminish faster compared with the long-wavelength patterns. Specifically, the amplitude reduction of the long-wavelength patterns follows the dc remanence curve rather closely, while the shorter patterns decrease in amplitude much more rapidly than that suggested by the remanence curve. The amplitude of L_2 was down to 50% of its initial value at 50 Oe below H_c, and was approximately down to 20% of its initial value at H_c. The L_2 signals were nearly extinguished even before reaching the average coercive field. By contrast, the L_1 patterns were diminished only by 50% at H_c and required about 50 Oe higher than the coercivity to decrease the amplitude to 20%. Thus, it appears that the difference in demagnetizing fields between the long and short patterns introduced a spread of nearly 100 Oe in the required field to produce the same amount of signal reduction. At the highest fields, however, the magnetization and the associated demagnetizing fields decrease so that the spread between the two curves diminishes at fields higher than H_c.

4.2. Trackwidth reduction

Concurrent with the decrease in overall pattern amplitude, we find a more rapid contrast reduction near the track edges as opposed to those at the interior of the tracks. This yields an apparent shortening of the trackwidth with increasing fields. While an overall reduction in the magnetization strength can reduce the local fields and may similarly show an artificial trackwidth reduction, we believe that this observed effect is indicative of the relative ease by which moments near the track edges can be rotated by the fields. A plausible explanation is hinted by considering the image of a similar medium in Fig. 4(a). This figure shows a single 12 μm wavelength pattern which has been imaged such that the trans-

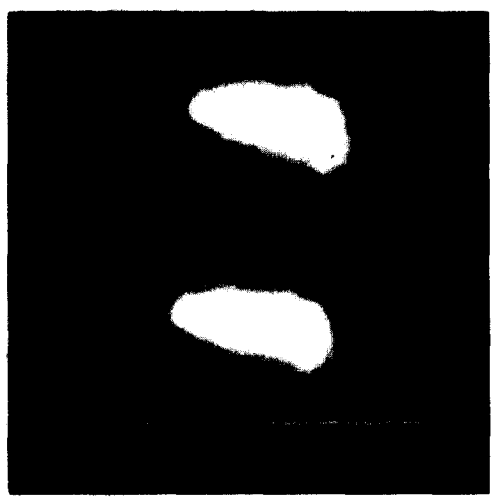

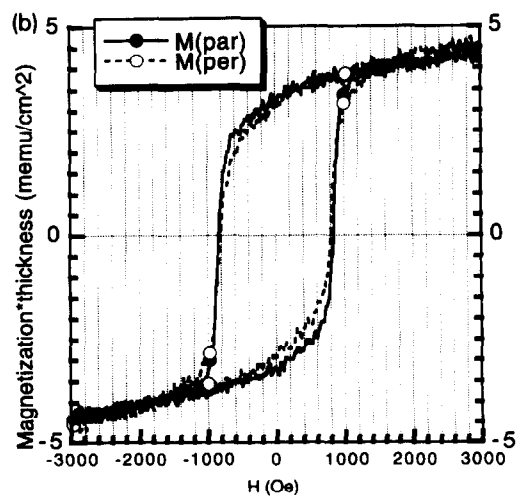

Fig. 4. Track-edge structures on a thin-film recording medium. Cross-track (H_y) and vertical field (H_z) components reveal the existence of a transverse magnetization component. Inset: measured magnetization curves.

verse and in-plane field component (H_y) together with the vertical component (H_z) were preferentially detected. In addition to the features in the interior of the track, there exists localized bright and dark bands along the edges. These features reveal the existence of side-written transverse magnetization components at the track edges [11]. These bands are believed to arise from the effect of the side fringing field generated by the recording head during the writing process. Micromagnetic modeling has predicted their existence, and their strength is believed to depend crucially on the relative in-plane anisotropy of the media [13]. They readily appear for a weakly oriented medium. Fig. 4(b) also shows the macroscopic M–H loop, which affirms that this sample was isotropic. The previous sample similarly shows an orientation ratio which is small in comparison with the orientation ratios associated with ordered media [13]. It is then reasonable to assume that a similar transverse band existed in that medium as well. At the edges, the magnetic moments need only to be rotated by 90° which can be achieved at a much lower field than that needed to accomplish a 180° magnetization reversal in the interior of the tracks. Hence, rotation occurs first at the outer edges and coupling facilitates the rotation of adjacent areas in the interior of the tracks. An alternative mechanism for the observed trackwidth reduction may be due to the formation of flux closure structures at the edges. Under the action of a dc field, the moments at the edges can rearrange themselves to form flux closure structures which yield a vanishing magnetization. This is in contrast with the previous case where the spins along the edges are all reoriented in the direction of the applied field. However, if this were the case, then preferential erasure at the corners formed by the transitions and the edges would occur since these corners are most susceptible to vortex formation. This has not been observed. Furthermore, this type of medium as shown in Fig. 1(b), exhibits positive interparticle interaction and the alignment of spins are energetically favorable [14,15]. Hence, it is quite likely that the trackwidth reduction is not due to vortex formation at the edges but rather, by the 90° rotation of the moments at the edges.

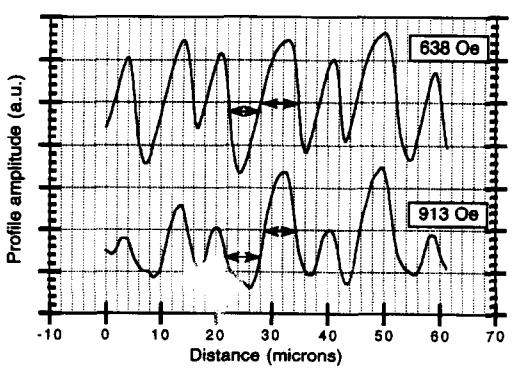

Fig. 5. Lineshape profile for the middle tracks in images A and D in Fig. 2.

4.3. Bit length expansion and contraction

The displacement of the boundaries between the dark and bright contrast areas indicates that the local magnetic field or equivalently, the magnetization distributions either expand or diminish in size in response to dc fields below the coercivity. This is best observed by viewing the sequence of images at video rates and watching the magnetic field lapse evolution of the patterns. This is somewhat reminiscent of domain expansion in magnetic thin films as they traverse various locations along their B–H loops. However, in contrast with the reversible domain motion in crystalline ferromagnetic samples, the observed domain expansion in this case is associated with the sample remanent state. This is an irreversible process and the motion of the boundaries correspond to various points along the dc demagnetization remanence curve. By comparing the images in Fig. 2A–D with the dc remanence curve in Fig. 1, we deduce that within this range of applied fields, most of the magnetic moments that switch (apart from the guard bands) were those near the transition regions. The line profiles in Fig. 5 provide a hint as to how this is accomplished. The unperturbed configuration in image (A) and the field-altered image (D) shows approximately 1 to 1.5 μm increase in the length of the dark contrast regions in D relative to that in A and accompanied by a similar decrease of the lengths of the bright-contrast areas. (For clarity, the arrows in Fig. 5 emphasize specific areas for comparison.) More important, the lineshape behavior shows that changes in the transition length parameter occur during erasure. Specifically, the lineshapes evolved from being asymmetric (right-skewed) in the unperturbed patterns into becoming more or less

symmetric after applying fields close to coercivity. The movement of the peaks (and bottoms) toward the center suggests that the effective transition length parameter increases [16]. Since this system prefers to be in a magnetized rather than a demagnetized state the transition-broadening mechanisms which cause the local magnetization to vanish (i.e. vortex formation) are unfavorable so that it is highly probable that the growth of zig-zag domain walls at the transition regions are primarily responsible for the observed transition length broadening. In other words, 'domain' movement proceeds as the antiparallel magnetic moments reverse direction, which causes the expansion of one magnetization direction at the expense of the other.

Finally, we comment on the possibility that this behavior might be an artifact of the measurement. One way that a spurious movement in the transition zones can occur is when the instrument readjusts the midpoint of the transition region between two neighboring opposite magnetizations. This may occur since the contrast mechanism in this technique depends upon the relative differences between neighboring opposite magnetizations and can not measure the absolute strength of the local magnetization. This is the reason why the contrast for both dark and bright areas diminish equally even if only one magnetization direction is being reversed by the external field. This virtual transition shift can be estimated by calculating the location of the transition point had it not been readjusted to be at the midpoint. For simplicity, assuming a sine function for the patterns, $y = \sin(2\pi x/\lambda)$, image D requires an offset of 95 nm to align its lowest point with that in A. This is half the difference in the peak amplitude between A (± 223 nm) and D (± 128 nm). It is easy to see that virtual movement, x', is given by $\lambda/2\pi \sin^{-1}(95/223)$, where λ is the wavelength of a specific pattern. For the long bit patterns $\lambda = 12$ μm, $x' = 0.84$ μm, while for $\lambda = 6$ μm, $x' = 0.42$ μm. Hence, while the wavelength dependence of the expansion is not observed in our results, these values nevertheless represent lower limits on the detectability of transition motion with our technique.

4.4. Cluster switching

For fields at and above the coercivity, the most dominant effect is the switching of clusters which results in a residual distribution of unswitched magnetic islands at any given field. It would be interesting to quantify the distribution of these clusters at progressively increasing applied fields since such a distribution may be correlated with the switching field distribution in the presence of interparticle interaction as well as the dispersion of the local anisotropy fields. Unfortunately, the resolution of this technique is inadequate to ascertain the changes in the distributions for small applied field increments. Hence, while distinct disappearance of clusters can be observed between the large field increment of 55 Oe between 2D and E, the diminution is much more gradual at finer field increments. Similarly, since this technique is, strictly speaking, sensitive to the magnetic field rather than the local magnetization distribution, so that the switching of minute clusters may introduce only a minimal variation in the image contrast. Nevertheless, Figs. 2 D–H show specific areas that disappear as others tenaciously persist. For fields close to the coercivity, there appears more of a tendency for clusters located near the track edges to switch prior to those in the interior regions. This may be a residual effect of the reduction in trackwidth described above. At higher fields, however, the remaining 'hard' areas do not seem to have direct correlation with their location across the track. It is equally likely to find unswitched clusters at the centers of the tracks as it is near the edges. In addition, there were cases where the contrast of a specific area diminishes partially at the low fields, but remains at much higher fields. The tenacity of specific areas against reversal do not have direct correlations with topographical features such as machine grooves, scratch marks or surface pits. It appears that this cluster distribution reflects the intrinsic switching characteristic of the grains of the medium and that grains of varying switching fields are distributed more or less randomly across the surface.

4. Conclusions

Based on these results, we summarize the behavior for pattern erasure for this system. At about 100 Oe below H_c, the moments at the edges are the first to undergo 90° rotations towards the direction of the

field which leads to reduction of the pattern trackwidth. Soon afterwards, the magnetic moments at the transition regions which were initially opposite to the applied field switch in the direction of the field, which causes the expansion of areas favorable to the applied field. Both of these processes continue up to the coercive field. At the dc coercive remanent field, the moments from two growing domains begin to coalesce at various localized areas leading to a 'punch through' of neighboring domains. As a consequence, the patterns break up into randomly distributed unswitched islands. The random distribution of the switched clusters on the medium reflects the distribution of the switching fields of magnetic moments which are distributed uniformly over the surface. Switching continues at fields above H_{dc} as the islands gradually disappear.

Finally, it is worthwhile mentioning that the erasure mechanisms depend crucially upon the macroscopic parameters of the medium. For instance, trackwidth reduction at the onset cannot be expected to markedly occur with a highly oriented medium since the cross-track edge magnetization in this case is negligibly small [13]. Similarly, a medium with negative interparticle interaction favoring demagnetization (i.e. particulate tape media [7]) can be expected to have transition width broadening caused by the formation of flux closure structures. Likewise, the squareness of the B–H loop will determine both the rate at which erasure proceeds as well as the uniformity of the distribution of cluster switching. The direct correlation between macroscopic and microscopic erasure characteristics can be understood by performing a systematic study of a wide variety of magnetic recording media subjected to both dc and ac external fields. Those measurements, in conjunction with theoretical modeling, will form the basis of a thorough understanding of the mechanisms of pattern elimination in magnetic media. Finally, it would be a natural extension of this work to observe the evolution of the patterns with enhanced resolution and in the presence of an external field. This will provide direct correlation of microscopic processes occurring at specific locations along the hysteresis loop.

Acknowledgements

We wish to thank N. Bartelt for his assistance in data analysis and computer graphics support; and A. Kratz, M. Shih, C. Buehler and S. Silliman for their help in developing the apparatus, as well as collection and data analysis.

References

[1] A. Lyberatos, E.P. Wohlfarth and R.W. Chantrell, IEEE Trans. Magn. 21 (1985) 1277.
[2] E.R. Burke and D.R. Sanders, IEEE Trans. Magn. 21 (1985) 1374.
[3] R.R. Katti, F. Servan-Schreiber and M.H. Kryder, J. Appl. Phys. 61 (1987) 4037.
[4] K.C. Weisen, R.R. Katti, S.H. Charap and M.H. Kryder, J. Appl. Phys. 63 (1988) 3378.
[5] R.D. Barndt, A.J. Armstrong, H.N. Bertram and J.K. Wolf, IEEE Trans. Magn. 27 (1991) 4978.
[6] B.D. Martin and D.N. Lambeth, IEEE Trans. Magn. 28 (1992) 3276.
[7] L. Lekawat, G.W.D. Spratt and M.H. Kryder, IEEE Trans. Magn. 29 (1993) 3628.
[8] P. Kelly, K. O'Grady, P. Mayo and R.W. Chantrell, IEEE Trans. Magn. 25 (1989) 3881.
[9] R.D. Gomez, E.R. Burke, A.A. Adly and I.D. Mayergoyz, Appl. Phys. Lett. 60 (1992) 906.
[10] I.D. Mayergoyz, A.A. Adly, R.D. Gomez and E.R. Burke, J. Appl. Phys. 73 (1993) 5796.
[11] R.D. Gomez, E.R. Burke and I.D. Mayergoyz, J. Appl. Phys. 75 (1994) 5910.
[12] R.D. Gomez, A.A. Adly, I.D. Mayergoyz and E.R. Burke, IEEE Trans. Magn. 29 (1993) 2494.
[13] J.G. Zhu, X. Ye and N. Arnoldussen, IEEE Trans. Magn. 28 (1992) 2716.
[14] J. Heidmann, T.A. Nguyen, T. Yogi, S.E. Lambert and V.S. Speriousu, J. Appl. Phys. 69 (1991) 7731.
[15] I.A. Beardsley and J.G. Zhu, IEEE Trans. Magn. 27 (1991) 5037.
[16] R.D. Gomez, E.R. Burke, A.A. Adly, I.D. Mayergoyz, J.A. Gorczyca and M.H. Kryder, J. Appl. Phys. 73 (1993) 6180.